Discrete solitons in nonlinear zigzag optical waveguide arrays with tailored diffraction properties

Nikos K. Efremidis and Demetrios N. Christodoulides
Department of Electrical and Computer Engineering, Lehigh University, Bethlehem, Pennsylvania 18015
(Received 18 January 2002; published 2 May 2002)

We show that the discrete diffraction properties of a nonlinear optical zigzag waveguide array can be significantly modified, by exploiting the topological arrangement of the lattice itself. This introduces extended interactions (beyond nearest neighbors), which, in turn, affect the lattice dispersion relation within the Brillouin zone. As a result of this band alteration, we demonstrate that altogether different families of discrete soliton solutions are possible, which are stable over a wide range of parameters. In the regime where instabilities occur, all scenarios are considered in detail. By appropriately engineering the geometrical configuration of the array we find both standing and traveling diffraction-free beams. Our method opens opportunities for diffraction management that can be employed to generate low-power spatial discrete optical solitons.

DOI: 10.1103/PhysRevE.65.056607 PACS number(s): 42.65.Tg, 05.45.Yv, 42.65.Wi

I. INTRODUCTION

Discrete solitons in nonlinear lattices are, by nature, self-localized modes that owe their existence to the interplay between coupling and nonlinear effects. In the last few years, the study of discrete solitons (DS) has been a subject of intense investigation in several branches of science (see, for example, the review papers of Ref. [1]). Among the known discrete nonlinear differential equations describing such systems, the discrete nonlinear Schrödinger equation (DNLS) plays a prominent role. In particular, discrete solitons of the DNLS-type have been suggested in many diverse areas of physics such as, for example, in biology [2], nonlinear optics [3], in molecular crystals [4], atomic chains [5], as well as in dilute Bose-Einstein condensates [6].

In optics, nonlinear waveguide arrays [3] provide an excellent environment for the generation and the experimental observation [7] of discrete solitons. In this case, spatial DS are possible as a result of the balance between discrete diffraction (arising from linear coupling effects) and waveguide nonlinearity. So far, several aspects concerning the behavior of optical discrete solitons have been investigated [8–12]. These include, for example, DS dynamics [11] and interactions [8,9], as well modulational instabilities [13]. Other types of self-trapped states, e.g., optical vortices, have also been considered [14].

In a recent study, it was also shown that DS in two-dimensional networks of nonlinear waveguide arrays can be used to realize *intelligent functional operations* such as blocking, routing, logic functions, time gating, etc. [15]. In particular, this class of solitons can be all optically navigated anywhere in the nonlinear lattice. In this case, the array branches behave like ''soliton wires'' that guide a DS along preassigned paths [16]. Even more importantly, discrete solitons can be routed at array intersections using vector/incoherent interactions with other DS. In essence, these intersections act like discrete soliton *switching junctions* [17].

Another issue that has lately received considerable attention is that of *diffraction management* in waveguide arrays [18–20] and diffraction managed discrete spatial solitons [21]. In this respect, different families of discrete solitons can be obtained by exploiting the spatial dispersion properties of the lattice. Thus, unlike bulk solitons, both bright and dark DS can be observed in the same nonlinear material irrespective of the type of the Kerr nonlinearity (self-focusing or defocusing) [18–20]. What makes this possible is the fact that the diffraction behavior of the array can be essentially *inverted*. For example, dark (bright) DS can be observed in self-focusing (defocusing) arrays, provided that their ''momentum'' is located at the end of the Brillouin zone. In addition, the array diffraction can be minimized at the inflection point of the dispersion curve, thus allowing, to lowest order, diffraction-free propagation [18]. At this point, it is perhaps important to note that in arrays with linear topology (i.e., with all the waveguides lying in the same plane), the dispersion behavior of the lattice remains always the same. This in turn does not allow any flexibility in terms of shaping the discrete diffraction properties of the array. Thus, the question naturally arises as to whether one can *engineer* these properties by utilizing novel geometrical configurations in a two-dimensional environment.

In this paper we show that the discrete diffraction properties of a nonlinear optical waveguide array can be significantly modified, by exploiting the topological arrangement of the lattice itself. This introduces extended interactions (beyond nearest neighbors) that, in turn, affect the lattice dispersion relation within the Brillouin zone. For demonstration purposes, we apply our method in a zigzag array that can exhibit, in addition, strong second-order couplings. As a result of this band alteration, we demonstrate that completely different families of discrete soliton solutions are possible in such arrays which are stable over a wide range of parameters. These include staggered (π out of phase) bright DS in self-focusing media as well as dark staggered DS in defocusing systems. In the regime where instabilities occur, all scenarios are considered in detail. More specifically, we find that in a certain parameter space, in phase bright solitons (in self-focusing arrays) can exhibit bistable behavior whereas bright staggered DS can disintegrate as a result of oscillatory instabilities. In addition, we show that for certain configurations, discrete diffraction effects (up to third order) can be eliminated. Our method opens up opportunities for diffrac-

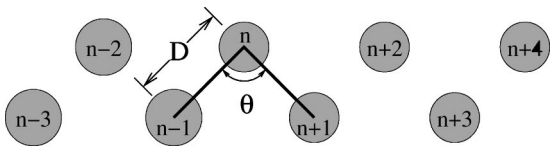

FIG. 1. A zigzag array of coupled optical waveguides.

tion management that can be employed to generate low-power discrete spatial solitons.

II. PHYSICAL MODEL

Figure 1 depicts an array of optical waveguides in a zigzag arrangement. In this array, D is the distance between ''nearest'' neighbors and θ is the angle between the lines connecting the nth element of the array with its neighbors $(n\pm1)$. Because of this new topological configuration, it is also essential that one also considers linear coupling effects between the nth site and its second-order neighbors $(n\pm2)$. From Fig. 1, these latter elements are separated by a distance $D_2=2D\sin(\theta/2)$. As we will see, when $\theta=180°$, the second-order interactions are extremely weak and as a result the physical problem is reduced to that of a DNLS (with only nearest-neighbor couplings). However, by decreasing the value of θ, second-order coupling effects start to become significant and thus they have to be included in the theoretical model. In this case, the underlying physical problem is described by the following nonlinear discrete differential equation [3]:

$$i\frac{dE_n}{dz}+\beta E_n+c_1(E_{n+1}+E_{n-1})+c_2(E_{n+2}+E_{n-2}) + \frac{k_0n_2}{2}|E_n|^2E_n=0, \tag{1}$$

where β is the propagation constant of each waveguide, and c_1, c_2 are, respectively, the first- and second-order coupling coefficients. E_n represents the modal field amplitude at site n, $k_0=2\pi/\lambda_0$, n_2 is the nonlinear Kerr coefficient of the material and z is the propagation distance along the array. In the particular case where the waveguides are of the step-index-type, the coupling constant between two such sites (separated by distance R) is given by [22]

$$c=\frac{\sqrt{2\Delta}}{\rho}\frac{U^2}{V^3}\frac{K_0(WR/\rho)}{K_1^2(W)}, \tag{2}$$

where ρ is the radius of the waveguide core, $\Delta=(n_c-n_s)/n_c$ is the waveguide index difference, and $V=k_0\rho n_c\sqrt{2\Delta}$ is the dimensionless V number involved in the eigenvalue problem describing the fundamental mode LP_{01} of the waveguide, e.g., $UJ_1(U)/J_0(U)=WK_1(W)/K_0(W)$. In this last equation, $U=\rho(k_0^2n_c^2-\beta^2)^{1/2}$, $W=\rho(\beta^2-k_0^2n_s^2)^{1/2}$, where $K_l(x)$ and $J_l(x)$ are Bessel functions of order l and n_c, n_s are the core and cladding refractive indices, respectively. The propagation constant β can then be determined from the eigenvalue problem by keeping in mind that $V^2=U^2+W^2$. The coupling coefficients, c_j, $(j=1,2)$ are then found from Eq. (2) by replacing R with D, D_2, respectively. By employing the transformations, $E_n=Gu_n\exp\{i[\beta z_0+2(1+\alpha)]\zeta\}$, $\zeta=z/z_0$, in Eq. (1), we obtain the following dimensionless form of Eq. (2):

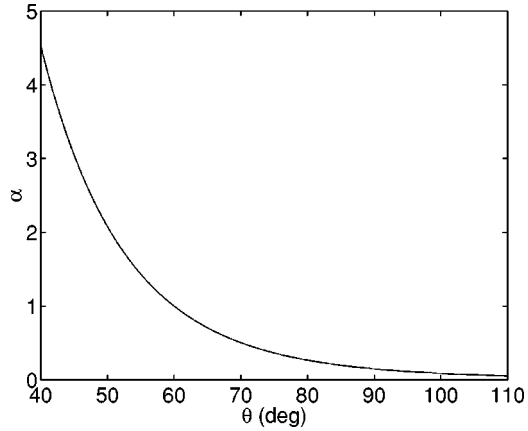

FIG. 2. The variation of α as a function of θ for a zigzag optical waveguide array.

$$i\frac{du_n}{d\zeta}+\Delta_1u_n+\alpha\Delta_2u_n+|u_n|^2u_n=0, \tag{3}$$

where the operators Δ_j, $(j=1,2)$ are defined by the relations $\Delta_1u_n=u_{n+1}+u_{n-1}-2u_n$, $\Delta_2u_n=u_{n+2}+u_{n-2}-2u_n$. u_n is the dimensionless field amplitude, ζ is a normalized propagation distance with respect to the coupling length $z_0=1/c_1$, $G=\sqrt{2c_1/k_0n_2}$ is a characteristic electric field amplitude, and α signifies the relative strength between the first and the second neighbor couplings, i.e.,

$$\alpha=c_2/c_1=K_0(WD_2/\rho)/K_0(WD/\rho). \tag{4}$$

For demonstration, let us assume that $\lambda_0=1.5$ μm, $n_c=1.5$, $\Delta=2\times10^{-3}$, $\rho=5.3$ μm, $D=15.9$ μm so that $D_2=31.8\sin(\theta/2)$ (in μm), $V=2.1$, $U=1.561$, and $W=1.405$. For this set of values Fig. 2 depicts the variation of α as a function of θ as it can be obtained from Eq. (4).

The conserved quantities of Eq. (3) are the total power in the array

$$P=\sum|u_n|^2, \tag{5}$$

as well as the Hamiltonian

$$H=\sum\left[|u_n-u_{n-1}|^2+\alpha|u_n-u_{n-2}|^2-\frac{1}{2}|u_n|^4\right] \tag{6}$$

from where one can obtain the equations of motion [Eq. (3)] via $i\dot{u}_n=\partial H/\partial u_n^*$.

It is important to note that Eq. (3) can also be analyzed by considering the transformation $u_n=\phi_n\exp(iqn)$, where q represents a phase shift among successive discrete sites and, in

essence, translates the spatial carrier wave number within the Brillouin zone. In this new representation Eq. (3) takes the form

$$i\dot{\phi}_n+(\phi_{n+1}e^{iq}+\phi_{n-1}e^{-iq}-2\phi_n)+\alpha(\phi_{n+2}e^{2iq}+\phi_{n-2}e^{-2iq}-2\phi_n)+|\phi_n|^2\phi_n=0. \quad (7)$$

If we define a normalized coordinate $\xi=s/D$, where s is the actual transverse skew coordinate along the zigzag path, then, in the so-called continuous approximation, Eq. (7) becomes

$$i\phi_\zeta+2\sum_{m=0}^{\infty}\frac{1}{(2m)!}[\cos q+\alpha 2^{2m}\cos 2q]\frac{\partial^{2m}\phi}{\partial\xi^{2m}}+2i\sum_{m=0}^{\infty}\frac{1}{(2m+1)!}[\sin q+\alpha 2^{2m+1}\sin 2q]\frac{\partial^{2m+1}\phi}{\partial\xi^{2m+1}}-2(1+\alpha)\phi+|\phi|^2\phi=0, \quad (8)$$

where $\phi_\zeta=\partial\phi/\partial\zeta$, etc. For broad enough beams, Eq. (8) can be approximated by keeping only the first terms of the Taylor series. In this case, if we employ the gauge transformation, $\phi=\psi\exp[2i\zeta(\cos(q)+\alpha\cos(2q)-1-\alpha)]$, and retain up to fourth-order diffraction effects, then this latter equation takes the form

$$i(\psi_\zeta+v_g\psi_\xi)+d_2\psi_{2\xi}+id_3\psi_{3\xi}+d_4\psi_{4\xi}+|\psi|^2\psi=0, \quad (9)$$

where

$$v_g=2(\sin q+2\alpha\sin 2q), \quad (10)$$

$$d_2=\cos q+4\alpha\cos 2q, \quad (11)$$

$$d_3=\frac{1}{3}(\sin q+8\alpha\sin 2q), \quad (12)$$

$$d_4=\frac{1}{12}(\cos q+16\alpha\cos 2q). \quad (13)$$

In Eq. (10) v_g stands for the wave's spatial group velocity, and d_j, $(j=2,3,4)$ represent the second-, third-, and fourth-order diffraction effects in the array, respectively. Finally, one may also notice that Eq. (3) is in fact identical to the following integro-differential equation:

$$i\phi_\zeta+\frac{1}{\pi}\int\int\{\cos(q+k')+\alpha\cos[2(q+k')]\}\times\phi(\eta,\zeta)e^{ik'(\xi-\eta)}d\eta dk'-2(1+\alpha)\phi+|\phi|^2\phi=0. \quad (14)$$

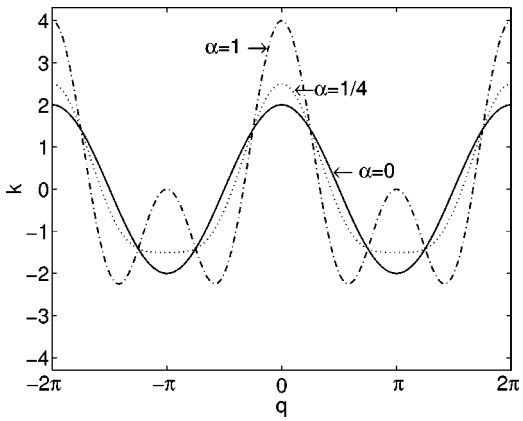

FIG. 3. The linear part of the dispersion relation for $\alpha=0,1/4,1$.

III. DISPERSION RELATION AND MODULATION INSTABILITY

To obtain the dispersion relation of this zigzag nonlinear lattice we use the "plane wave" solution $u_n=Ae^{i(kz+qn)}$, where the wave number k satisfies

$$k=2\cos q+2\alpha\cos 2q+A^2-2(1+\alpha), \quad (15)$$

and again q represents the phase shift among successive sites and plays the role of "particle momentum." The shifted [by $2(1+\alpha)$] linear part of the dispersion relation, $2(\cos q+\alpha\cos 2q)$, is depicted in Fig. 3 for three different values of α, namely, $\alpha=0,1/4,1$. Note that the first Brillouin zone is defined in the domain $-\pi\leqslant q\leqslant\pi$. First, we would like to discuss the properties of this linear dispersion curve. To begin with, let us examine the behavior of the dispersion relation at the DNLS limit, i.e., when $\alpha=0$. When q lies in the range $-\pi/2<q<\pi/2$ the curvature of the dispersion relation is negative $[k''(q)<0]$, and, as a result, the effective diffraction of the array is "anomalous." On the other hand, when $\pi/2<|q|\leqslant\pi$ the curvature is positive $[k''(q)>0]$, and the effective dispersion of the array is now "normal." In this case $(\alpha=0)$ the dispersion curve attains a maximum at $q=0$, and, as a matter of fact, the bright soliton solutions of the DNLS reside at this point with eigenvalues that lie above this curve (in the band gap). Each member of this family of bright solitons is characterized by the separation distance between the eigenvalue of the solution and the edge of the band. Furthermore, these solutions have altogether different properties depending on their position inside the band gap. When the eigenvalue is relatively close to the edge of the band, the bright soliton solutions are broad (occupying many lattice sites), they possess a narrow spatial frequency spectrum, and, as a result, the long wavelength approximation of the dispersion relation is valid. In this regime the dispersion relation can be described within the parabolic approximation and thus Eq. (3) is equivalent to a continuous nonlinear Schrödinger equation [Eq. (9) with $d_3=d_4=0$]. The soliton solutions with wave numbers positioned very deep inside the band gap represent highly nonlinear "defect" states occupying, in essence, 1–3 lattice sites. We can also notice that at

the edge of the zone, i.e., when $q=\pi$, the dispersion curve reaches a minimum. Here, since the dispersion is normal, π out of phase dark soliton solutions (staggered) exist inside the band gap as a result of this band minimum [20]. The form of these dark soliton solutions can be easily obtained, if we follow procedures similar with those already outlined in this section for bright solitons.

However, as clearly seen in Fig. 3, the properties of the dispersion diagram within the Brillouin zone can be drastically altered for appreciable values of the second-order-coupling strength α. A close inspection of the dispersion diagram can provide valuable hints concerning the possible types of soliton solutions and their properties. More specifically, at the base of the Brillouin zone, i.e., when $q=0$, we notice that as the value of α increases, the dispersion curve becomes narrower (the absolute value of the second derivative of the dispersion relation increases linearly with α); this, in turn, leads to broader bright soliton solutions compared to those with smaller values of α for the same power P. On the other hand, at the edge of the zone, $q=\pi$, the dispersion relation exhibits a very different behavior depending on the value of α. In particular, for α's located inside the region $[0,1/4)$ the second derivative of the dispersion curve, $k''(\pi)$, is always positive and, therefore, the lattice dispersion is normal. In the case $\alpha=1/4$ the second-order dispersion is zero and the first nonzero contribution comes from the fourth-order dispersion that happens to be positive. When α is above 1/4, the value of $k''(\pi)$ becomes negative, and as we will show *a completely different family of bright staggered solitons in self-focusing arrays exists*. This latter class of solutions has no counterpart whatsoever in standard arrays with only first-order couplings described by the DNLS. As the value of α increases above 1/4 the dispersion curve becomes narrower and, thus, the bright soliton solutions become broader.

Our previous conclusions can be further substantiated by considering the modulational instability of the plane wave solution of Eq. (3) with respect to small perturbations. As it is well known, the existence of modulational instability is closely related to the presence of bright soliton solutions. More specifically, if the plane wave solution is unstable, it may then tend then to disintegrate into a sequence of bright solitons, i.e., loosely speaking the presence of modulational instability can be considered as a precursor to bright soliton formation. Perturbing the amplitude and the phase of the solution as $u_n=(A+B_n)\exp[i(k\zeta+qn+\psi_n)]$, where B_n and the differences $\psi_{n+1}-\psi_n$ are assumed to be small and by applying the transformation $(B_n,\psi_n)\equiv(B,\psi)e^{i(K\zeta+Qn)}$ we obtain the following equation:

$$
\begin{aligned}
&[K+2\sin q\sin Q+2\alpha\sin 2q\sin 2Q]^2 \\
&\quad=8\left[\cos q\sin^2\frac{Q}{2}+\alpha\cos 2q\sin^2 Q\right] \\
&\quad\times\left[2\cos q\sin^2\frac{Q}{2}+2\alpha\cos 2q\sin^2 Q-A^2\right],
\end{aligned}
\tag{16}
$$

between the wave number K and the spatial frequency Q of the perturbations. A close inspection of Eq. (16), reveals the regions where modulational instability exists (i.e., where the plane wave is stable or unstable as a function of q and α). More specifically, at the base of the Brillouin zone, $q=0$, the continuous wave solution is unstable for all values of α. On the other hand, the stability of the plane wave solution at the edge of the Brillouin zone ($q=\pi$) depends on α; it is stable when $\alpha\leqslant 1/4$ and unstable otherwise. These results are in full agreement with the conclusions previously drawn from the linear dispersion diagram. Our results, i.e., Eq. (16), are in close agreement with those recently obtained in connection with nonlinear polymer chains [23].

IV. SOLITON SOLUTIONS AND THEIR STABILITY

We will now examine the existence and stability of the solitary wave solutions that we have already described qualitatively in the preceding section. It is by now well established that, for broad enough beams, this system is approximately described by a continuous nonlinear Schrödinger Equation [Eq. (9) when d_3 and d_4 are negligible], which is known to exhibit soliton solutions. However, in general (for moderately or strongly confined states), the solutions of the discrete Eq. (3) can only be obtained numerically. To do so, let us assume that the solution of Eq. (3) is having the form, $u_n=v_n\exp(i(\mu\zeta+qn))$, where v_n is the real amplitude of the nth site, μ is the eigenvalue, and the phase difference between adjacent sites, q, is equal to 0 or π. Equation (3) is now reduced to the following system of nonlinear algebraic equations:

$$
\begin{aligned}
&-\mu v_n\pm(v_{n+1}+v_{n-1})-2v_n+\alpha(v_{n+2}+v_{n-2}-2v_n)+v_n^3 \\
&\quad=0,
\end{aligned}
\tag{17}
$$

which will be solved numerically using a Newton's iteration scheme. The two cases of particular interest, i.e., $q=0$, π, corresponding to the $\pm$ signs, respectively, in Eq. (17), will be treated separately in the rest of this section.

A. At the base of the Brillouin zone: $q=0$

In the particular case where the phase difference between adjacent waveguides is zero, two different types of soliton solutions exist; those centered on a single site and those that are centered between two sites. Apart from that, these two solutions have a similar form (brightlike or darklike) as expected from the DNLS equation. As a matter of fact, for a fixed value of P, the energy (Hamiltonian) of the in-phase bright soliton solution centered on site is always less than the energy of the solution centered between two sites, and, therefore, the latter one is always transversely unstable. Consequently, we will restrict ourselves to the study of on site bright discrete soliton solutions [24].

The family of the in-phase bright solitons of Eq. (3) with $q=0$ are found numerically by solving the nonlinear system of Eq. (17). In Fig. 4 the power associated with these solutions, P, is depicted as a function of the eigenvalue μ for three different values of α. When $\alpha=0$, the $P(\mu)$ diagram

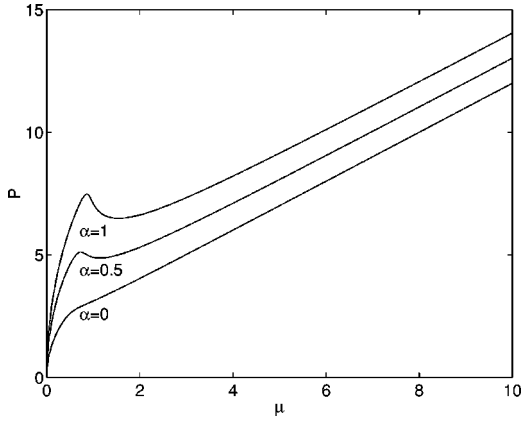

FIG. 4. Power P vs μ diagram of bright soliton solutions when $q=0$, and $\alpha=0,1/4,1$.

corresponds to the standard DNLS model. In this regime, approximate expressions for $P(\mu)$ can be obtained in the case of either weakly or strongly localized solutions, that is, in the continuous or the anticontinuous limit. More specifically, for relatively small values of P, the behavior of the $P(\mu)$ can be approximately described within the so-called nonlinear Schrödinger limit. In this case, using Eq. (5), the $P(\mu)$ curve can be approximately described by $P \approx 4\sqrt{(1+4\alpha)\mu}$. On the other hand, for large values of P, most of the power is confined in one waveguide, and, therefore, $P \approx \mu + 2(1+\alpha)$. The regions where these two approximations are valid can be easily seen in Fig. 4.

As a result of the long-range interactions, these solutions have interesting stability properties. A similar situation was encountered in Ref. [25] in nonlinear lattices with r^{-s} interactions. More specifically, when α is less than 0.26, the power P is always monotonically increasing with μ. On the other hand, for values of α greater than 0.26, a region (μ_1,μ_2) exists in which P is monotonically decreasing with μ, whereas, for all other subsequent values of μ, P is increasing. The $P(\mu)$ curves are associated with the stability of the soliton solutions through the Vakhitov-Kolokolov criterion [26] that has been shown to be also applicable in the DNLS equation [27]. According to this criterion, instability will be developed only when $\partial P/\partial\mu<0$, i.e., inside the region (μ_1,μ_2) when $\alpha \gtrsim 0.26$. From a different perspective, Fig. 4 can be interpreted as a $\mu(P)$ diagram. As it is known from elementary bifurcation theory, the stability properties of a system can change only when a bifurcation takes place. When $\alpha \lesssim 0.26$, $P(\mu)$ is monotonically increasing, i.e., no bifurcation occurs. We also know that the small amplitude solutions are stable since they are governed by the continuous NLS equation and, as a result, the whole curve is stable. In the other extreme, the stability of the strongly localized modes can also be proved analytically since, effectively, Eq. (3) reduces to a dynamical system with a few degrees of freedom (see, for example, Ref. [28]). When $\alpha \gtrsim 0.26$ we know that the upper and lower branches are stable, so, we expect (since the stable and unstable manifold alternate), that the second branch will be unstable. In the range where a given value of P corresponds to three different values of μ, two of these wave numbers, i.e., the minimum and the maximum values of μ, are stable, whereas the one in between is unstable.

We will now formally explore the linear stability of these in-phase bright soliton solutions by using Eq. (3). By perturbing the exact solution $u_n=v_n e^{i\mu\zeta}$, in a fashion $u_n=[v_n+(U_n+W_n)e^{i\Lambda\zeta}+(U_n-W_n)e^{-i\Lambda\zeta}]e^{i\mu\zeta}$, we obtain the following coupled eigenvalue problem:

$$L_1 W_n = \Lambda U_n, \quad L_2 U_n = \Lambda W_n, \tag{18}$$

where $L_1 W_n = -\mu W_n + \Delta_1 W_n + \alpha\Delta_2 W_n + v_n^2 W_n$ and $L_2 U_n = -\mu U_n + \Delta_1 U_n + \alpha\Delta_2 U_n + 3v_n^2 U_n$. When all the eigenvalues of the perturbation lie on the real axis the solution is stable, whereas, if an eigenvalue pair acquires a nonzero imaginary part the solution becomes unstable. The continuous spectrum can be found by linearizing Eq. (18), and substituing $c_n=(U_n+W_n)\exp(ip_a n)$, $d_n=(U_n-W_n)\exp(ip_a n)$, i.e.,

$$\Lambda = \pm[\mu + 2(1-\cos p_a) + 2\alpha(1-\cos 2p_a)],$$

We will show that the results stemming from the solution of the previous eigenvalue problem are in agreement with the previous analysis. To demonstrate this connection, we will describe how the eigenvalues of Eq. (18) change as a function of μ, when α is above the instability threshold. When μ is close to zero, the amplitude of the solution becomes very small, and, consequently, the discrete Eq. (3) is in the vicinity of the continuous NLS limit. In this case it is well known that two pairs of eigenvalues are located at the origin, corresponding to the even (with zero nodes) and an odd (with one node) eigenfunction. The first (even) mode is related to the invariance of the model to a phase shift, i.e., as it is proved by Noether's theorem, to the conservation of the power [Eq. (5)], whereas the second (odd) mode is related the translational invariance [the conservation of the momentum in the continuous approximation of Eq. (3), i.e., of the NLS equation]. As the value of μ increases the eigenvalues associated with the translational eigenmode bifurcate from the origin to the real axis and approach the edge of the continuous spectrum. This bifurcation is related with the loss of the mobility of the discrete soliton solutions as they become more localized on the nonlinear lattice. The other pair of eigenvalues remains at the origin as long as P is an increasing function of μ. When the slope of the $P(\mu)$ diagram becomes negative this pair of eigenvalues bifurcates from the origin to the imaginary axis, and, as a result, the soliton solution turns unstable. As long as the slope of $P(\mu)$ is negative, the eigenvalues remain on the imaginary axis. However, when the value of the slope is close to zero again, the eigenvalues return to the origin. This scenario is demonstrated in Fig. 5 for $\alpha=1$ and $q=0$ when $u_0=1.2,1.7,2.2$. The left column of Fig. 5 depicts the associated eigenvalue diagram, whereas the right one shows the corresponding evolution of the intensity of the discrete soliton. Figs. 5(a) and 5(b) were obtained at $u_0=1.2$, where the soliton is stable since all the eigenvalues lie on the real axis. On the other hand, the solution illustrated in Figs. 5(c) and 5(d) for $u_0=1.7$ is unstable, and exhibits bistability. In this case a pair of eigenvalues is

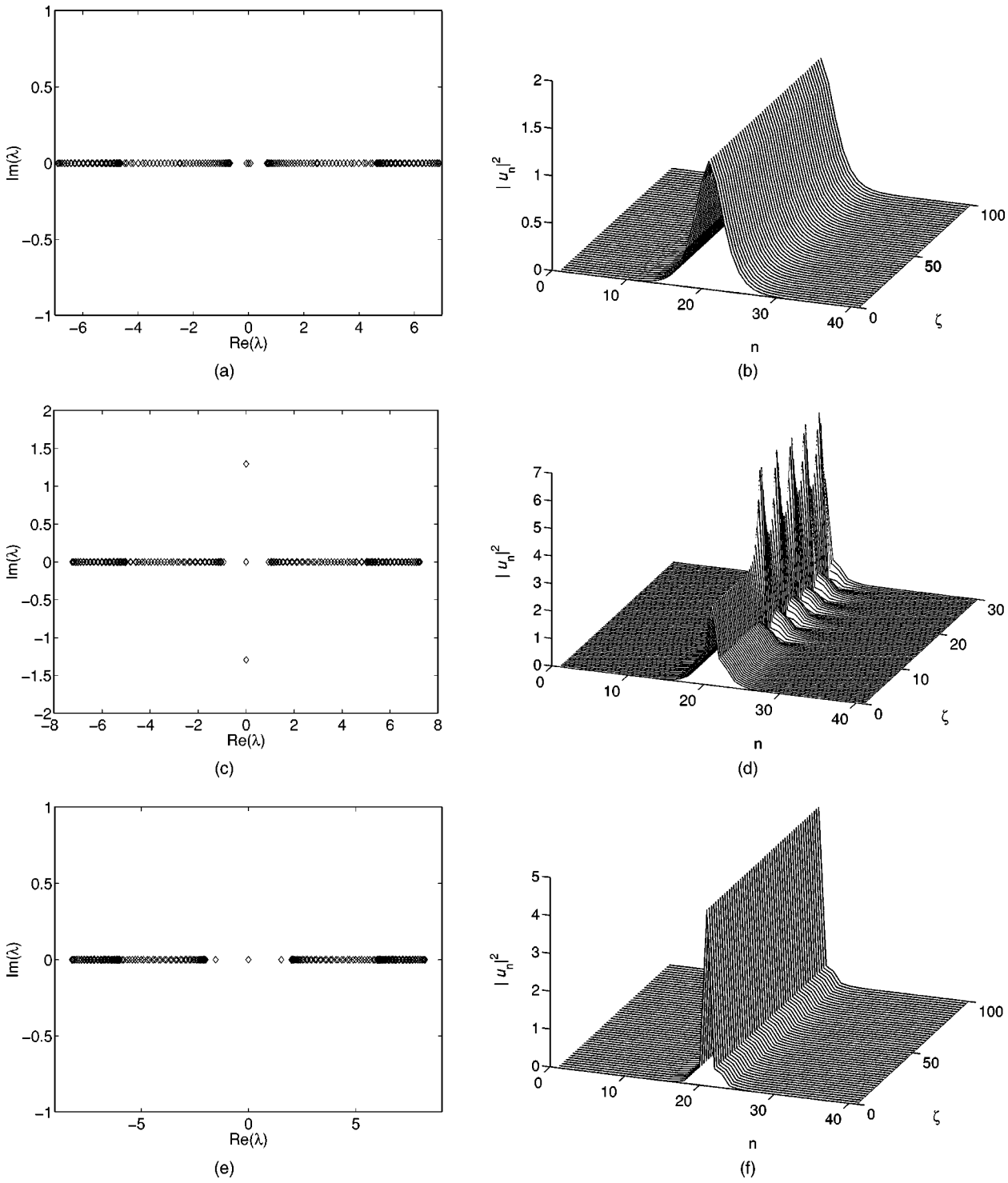

FIG. 5. Eigenvalue diagrams of in-phase bright soliton solutions ($q=0$) when $\alpha=1$, and for $u_0=1.2$, 1.7, 2.2 shown in (a), (c), (e) and the corresponding intensity evolution depicted in (b), (d), (f), respectively.

purely imaginary and is responsible for instabilities. This instability ceases to exist at higher amplitudes [see Figs. 5(e) and 5(f) where $u_0=2.2$], since all the eigenvalues are located on the real axis.

B. At the edge of the Brillouin zone: $q=\pi$

In this section we will explore the properties of staggered soliton solutions, i.e., $q=\pi$. As per our previous discussion in Sec. III we anticipate bright staggered soliton solutions to exist when $\alpha>1/4$. Again, we identify two different types of staggered bright solitons: (a) a symmetric mode, and (b) an antisymmetric mode. Figure 6 depicts both a narrow and a broad, symmetric and antisymmetric discrete soliton solution.

Between these two possible staggered solutions, the energy of the symmetric mode is always greater than the cor-

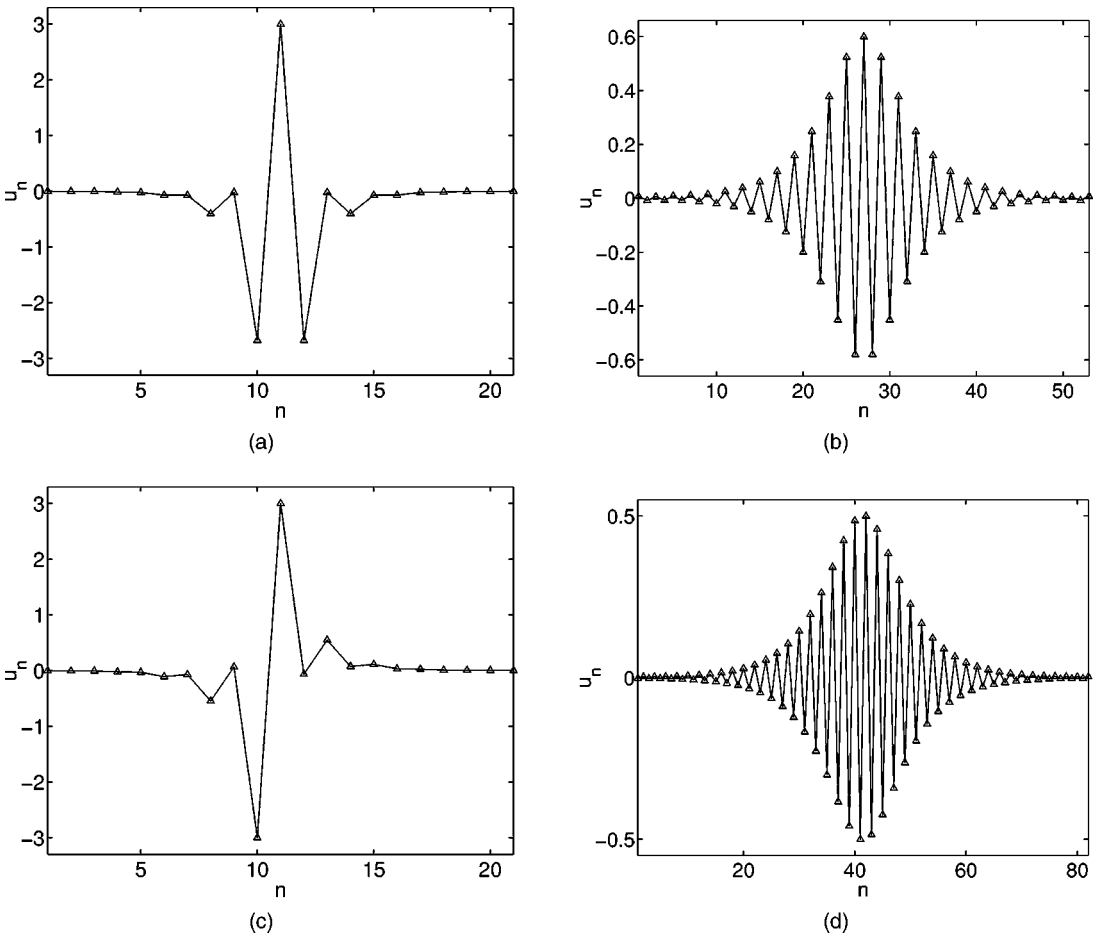

FIG. 6. (a), (b) symmetric and (c), (d) antisymmetric bright staggered soliton solutions. Figures (a), (c) correspond to highly localized solutions while (b) and (d) to relatively broad states.

responding value for the antisymmetric mode (for a fixed value of P and appreciable values of α). As a result, the symmetric mode happens to be transversely unstable. To study the stability properties of the antisymmetric solution, we will numerically solve the eigenvalue problem [Eq. (18)] where the linear operators are in this case $L_1 W_n = -\mu W_n - \Delta_1 W_n + \alpha \Delta_2 W_n + v_n^2 W_n$ and $L_2 U_n = -\mu U_n - \Delta_1 U_n + \alpha \Delta_2 U_n + 3 v_n^2 U_n$. Again, the continuous spectrum can be determined by linearizing the eigenvalue problem, and $\Lambda = \pm[\mu - 2(1-\cos p_a) + 2\alpha(1-\cos 2p_a)]$. Our numerical investigation shows that above a certain threshold of the maximum amplitude these solutions are stable. Figure 7(a) depicts the properties of the eigenvalue diagram associated with a stable solution when $\alpha = 1.4$ and the peak amplitude is 5. In this case we see a pair of eigenvalues located at the origin and another located on the real axis between the origin and the continuous spectrum. As a result the solution is stable as also demonstrated by its intensity evolution, Fig. 7(b). By decreasing the amplitude, the gap between the continuous spectrum and the latter pair of discrete eigenvalues is reduced as shown in Fig. 7(c) (for a peak amplitude equal to 4). This solution is again stable, as demonstrated in Fig. 7(d). Finally, when the amplitude is reduced below a certain threshold, the eigenvalue pair collides with the continuous spectrum and bifurcate into four eigenvalues with nonzero imaginary components [Fig. 7(e)] giving rise to an oscillatory type of instability [see also Fig. 7(f)].

Following the arguments of Sec. III, we have also found numerically staggered dark soliton solutions in the region $\alpha < 1/4$. The properties of these solutions happen to be very similar to those of the DNLS equation, i.e., when $\alpha = 0$, (see Refs. [20,29]). As the value of α increases inside the region $[0,1/4)$, the width of the dispersion curve becomes broader, and, as a result, the soliton solutions become narrower for the same power levels. In Fig. 8 we present the form of the centered on a site [Figs. 8(a) and 8(b)] and centered between two sites [Figs. 8(c) and 8(d)] dark soliton solutions when $\alpha = 0$ [Figs. 8(a) and 8(c)] and $\alpha = 0.2$ [Figs. 8(b) and 8(d)].

V. DIFFRACTION MANAGEMENT

In a recent study, it has been demonstrated that the discrete diffraction properties of a linear array can be altered as a function of the input phase difference q among successive waveguides [18]. In particular, it was experimentally verified that for $q = \pi/2$, the optical beam in a linear array can propagate almost undistorted, since, to leading order, the discrete diffraction is zero [i.e., from Eq. (11) $d_2 = 0$ when $q = \pi/2$ and $\alpha = 0$]. Furthermore, diffractionless propagation was also observed by eliminating, on average, the third-order dif-

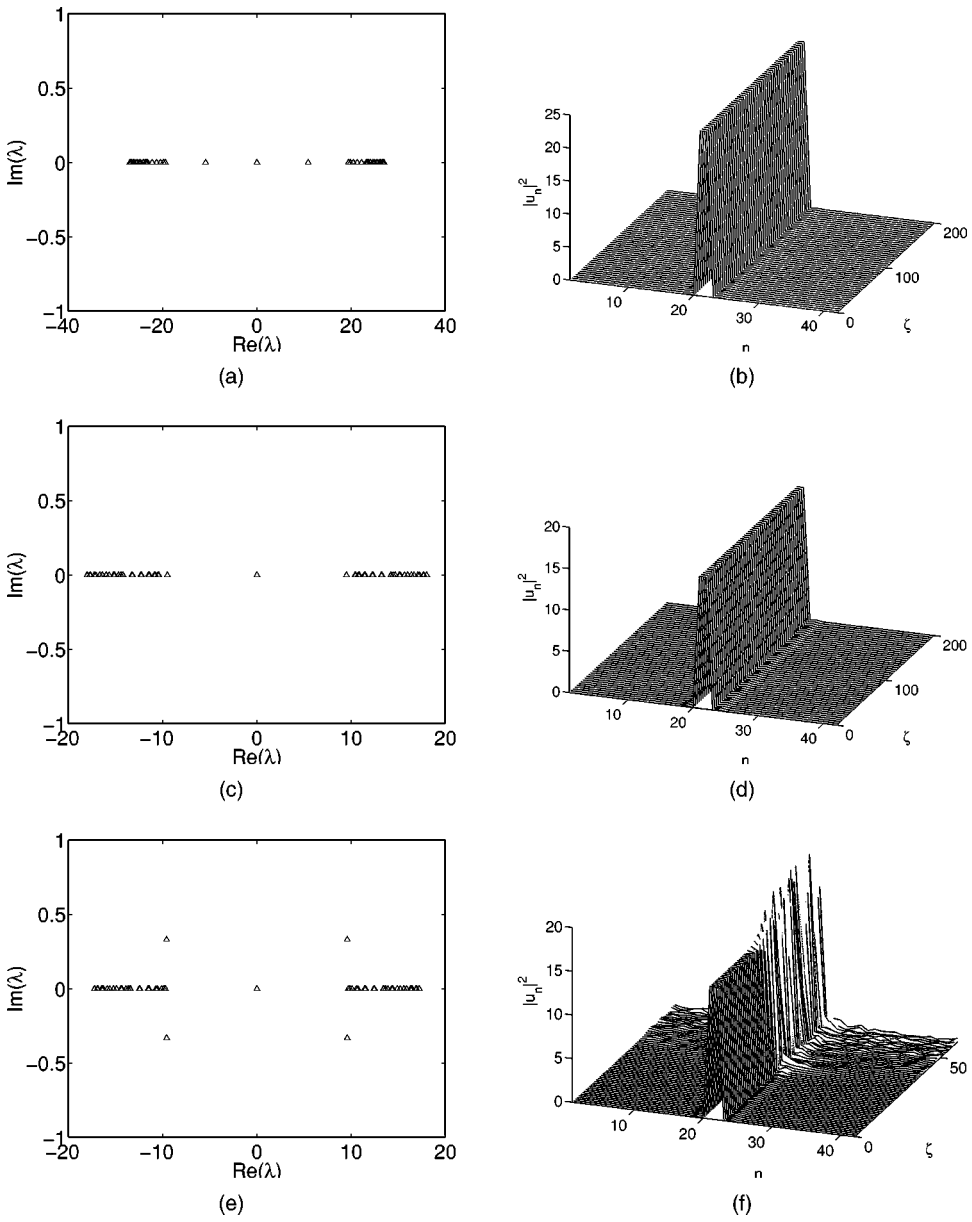

FIG. 7. (a), (c), (e) the eigenvalue diagram and, in (b), (d), (f), the corresponding propagation plots when $\alpha=1.4$ and the peak amplitude of the solution is 5, 4, and 3.9, respectively.

fraction using an alternating configuration (along z) of waveguide arrays.

In this section we will study how diffraction management can be implemented in the zigzag arrays proposed here. As previously noted the presence of second-order couplings (when $\alpha\neq 0$) can substantially modify d_2 since $d_2=\cos q+4\alpha\cos 2q$. The condition $d_2=0$ in fact corresponds to the inflection points of the dispersion curve (Fig. 3). From Eq. (11) the inflection points $\hat{q}$, where $d_2=0$, can be found, as a function of α, and are given by $\cos\hat{q}=[-1\pm\sqrt{1+128\alpha^2}]/16\alpha$. In Fig. 9, the group velocity [as given by Eq. (10)] that is associated with diffractionless beam propagation is displayed as a function of α. As we can see, for values of $\alpha<1/4$ diffractionless propagation can be achieved for only one value of q, while, for $\alpha>1/4$ two inflection points exist, each one corresponding to a different group velocity. Note that the case studied in Ref. [18] corresponds to $\alpha=0$ on the upper branch of our Fig. 9. Both v_g curves are increasing functions of α. However, it is important to point out that the group velocity displayed in Fig. 9 is related to the skew coordinate s that connects linearly all the consecutive sites of the array zigzag path. On the other hand, the actual propagation distance along the x coordinate (which is parallel to the line that connects a waveguide with its second neighbors) is related to s via $x=s\sin(\theta/2)$ and, as a result, the group velocity v_{gx} is reduced by a factor $\sin(\theta/2)$. It is interesting to note that, while in the first branch (solid curve) the normalized group velocity is always greater than 2, in the second branch (dashed curve) diffraction-free beam propagation is possible even for small values of v_g. Actually, when $\alpha=1/4$ and $q=\pi$ diffractionless propagation of a *standing beam* (since $v_g=0$) can be achieved. In this particular case, both d_2 and d_3 are zero and the first nonzero contribution comes from the fourth-order diffraction term. To verify this result, a beam of the form $u=\mathrm{sech}[0.35(n-n_0)/\sqrt{2}]\exp(iqn)$ was launched in such a linear array. Fig-

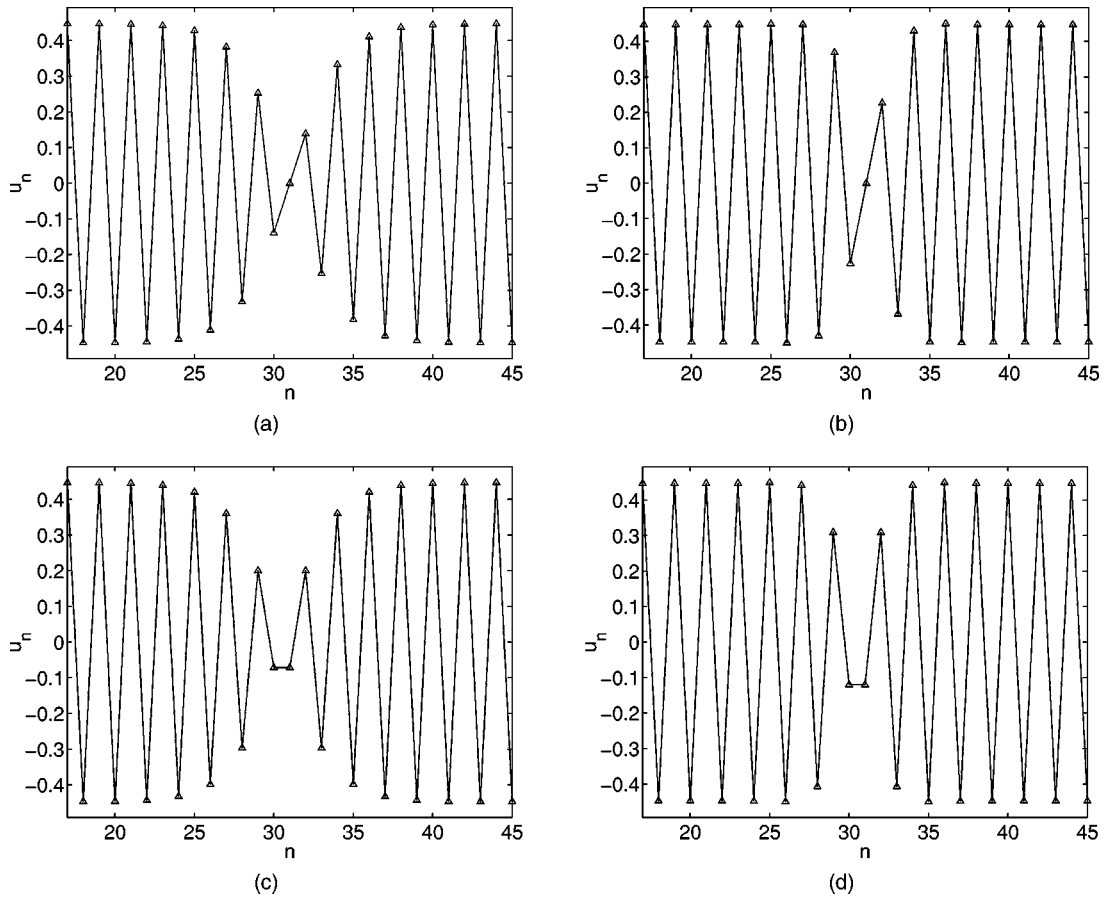

FIG. 8. Dark soliton solutions (a), (b) centered on a site and (c), (d) centered between two sites for (a), (c) $\alpha=0$ and (b), (d) $\alpha=0.2$.

ure 10 depicts the intensity profile of this beam at the input (solid curve) and at $\zeta=100$ when (a) $\alpha=0$, $q=0$ (dotted curve) (b) $\alpha=0$, $q=\pi/2$ (dashed dotted), and (c) $\alpha=1/4$, $q=\pi$ (dashed). For case (a) the peak intensity of the beam at the output is at least six times less than the one at the input, mainly as a result of second-order diffraction. In the second case (b), the initial phase tilt $q=\pi/2$ is responsible for the elimination of the second-order diffraction effects and the output peak intensity is reduced by 30%. In this case, the third-order diffraction is responsible for the asymmetric distortion of the beam. Finally, in case (c) the peak intensity is approximately 80% of the input, and any distortion in the beam profile is due to fourth- and higher-order diffraction terms.

The spatial dispersion or diffraction that a beam is experiencing during propagation in the bulk depends only on the refractive index of the material. In discrete systems, however, diffraction results from the coupling between the ele-

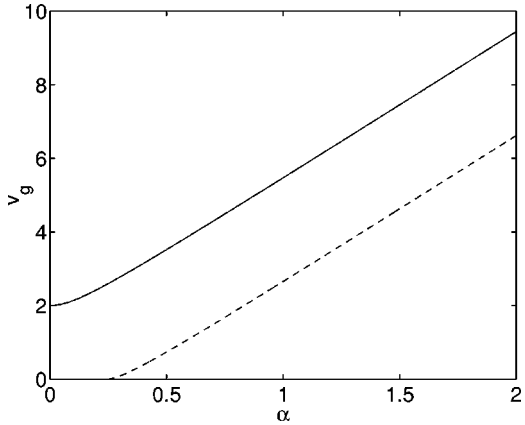

FIG. 9. Group velocity at the zero diffraction points. For α above 1/4 two different group velocity branches are allowed.

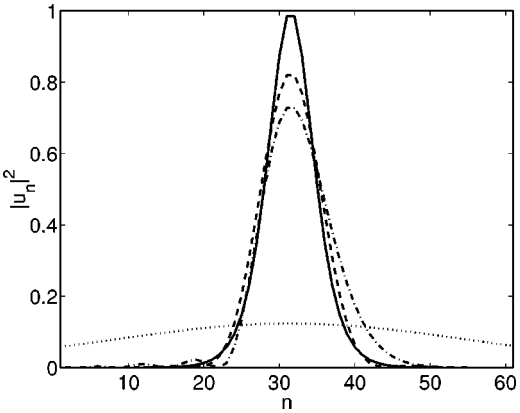

FIG. 10. The input (solid line) and the output intensity profiles of a beam after a propagation distance $\zeta=100$ when (a) $\alpha=0$ and $q=0$ (dotted line), (b) $\alpha=0$, $q=\pi/2$ (dashed-dotted line), and (c) $\alpha=1/4$, $q=\pi$ (dashed line).

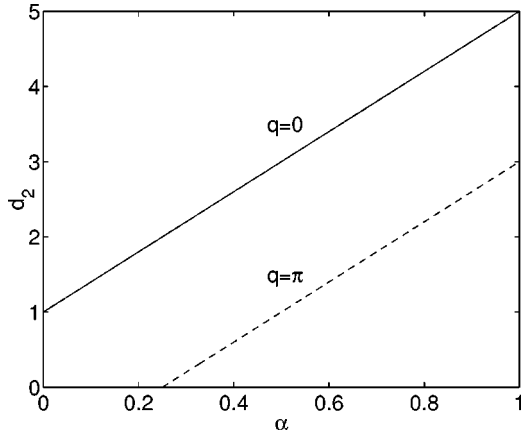

FIG. 11. The leading diffraction term d_2 of the waveguide array as a function of α for $q=0$ and π.

ments of the lattice. Consequently, different geometrical arrangements will have, in general, different diffraction properties. As Eq. (11) indicated, the diffraction can be tuned by adjusting the relative coupling strength α. As a result, solitons with specific peak intensities are possible, by appropriately engineering the relative coupling coefficient α. The diffraction of the zigzag array, d_2, is depicted in Fig. 11 as a function of α in the regimes where bright solitons can be supported. The two curves shown in the figure correspond to the cases $q=0$ and π. For these values of q the odd order diffraction terms, which are responsible for the asymmetric deformation of a soliton as well as for acceleration/deceleration effects, are zero. In both cases, the diffraction is an increasing function of α. For in-phase solitons d_2 attains its minimum value ($d_2=1$) at $q=0$. However, for staggered solitons ($q=\pi$), the leading diffraction term d_2 is zero when $\alpha=1/4$. Thus, staggered discrete solitons can exist even in media with relatively small values of nonlinearity.

VI. DEFOCUSING NONLINEARITY

Our formalism can also be used to obtain discrete soliton solutions in arrays with defocusing nonlinearity. In this case the optical field dynamics are described by

$$i\frac{du_n}{d\zeta}+\Delta_1 u_n+\alpha\Delta_2 u_n-|u_n|^2u_n=0. \tag{19}$$

When $\alpha=0$, Eq. (19) reduces to the defocusing DNLS. This equation is known to support in-phase dark soliton solutions at the base of the Brillouin zone ($q=0$), as well as out-of-phase (staggered) bright solitons at the edge of the Brillouin zone ($q=\pi$) [13,20]. The nonlinear dispersion relation of Eq. (19) is given by

$$k=2\cos q+2\alpha\cos 2q-A^2-2(1+\alpha). \tag{20}$$

Evidently, the linear part of Eq. (20) remains the same as in the self-focusing case (Fig. 3). Therefore, at the base of the Brillouin zone ($q=0$) one expects in-phase dark soliton solutions to exist. In addition, Fig. 3 demonstrates that as the value of α increases, the dispersion curve becomes narrower and, as a result, the dark soliton solutions that can be accommodated (at $q=0$) have to be broader for bigger values of α. At the edge of the Brillouin zone the sign of the second-order diffraction term d_2 of the array changes when $\alpha=1/4$. Following the same arguments we used in Sec. III, we anticipate that for values of α less than $1/4$ staggered bright soliton solutions should exist. This fact becomes apparent if one considers Eq. (9) when $q=\pi$ and the nonlinearity is of the defocusing type, i.e.,

$$i\psi_\zeta+(4\alpha-1)\psi_{2\xi}+\frac{1}{12}(16\alpha-1)\psi_{4\xi}-|\psi|^2\psi=0. \tag{21}$$

For broad enough solutions (in which case the fourth-order dispersion can be neglected) Eq. (21) reduces to the standard nonlinear Schrödinger equation with bright soliton solutions for $\alpha<1/4$ and dark solitons for $\alpha>1/4$. Of course in the discrete limit these solutions are of the staggered type since $q=\pi$. It is also noteworthy pointing out that Eq. (21) exhibits a bright solitary wave solution even in the presence of fourth order diffraction effects. This solution is given by [30]

$$\psi=A\,\mathrm{sech}^2(p\xi)e^{i\nu z}, \tag{22}$$

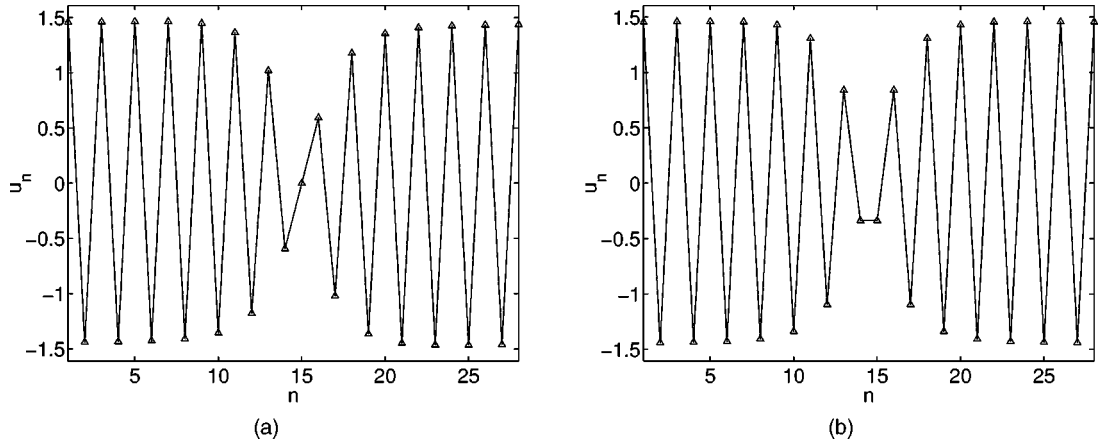

FIG. 12. A staggered dark soliton at the edge of the Brillouin zone (a) centered on a site and (b) centered between two sites.

where $A^2=(18/5)(1-4\alpha)^2/(16\alpha-1)$, $p^2=(3/5)(1-4\alpha)/(16\alpha-1)$, and $\nu=-(48/25)(1-4\alpha)^2/(16\alpha-1)$. This solution exists in the range $1/16<\alpha<1/4$. Notice that all the parameters of this solution are fixed for a given value of α. Finally, when $\alpha>1/4$ a new type of staggered dark soliton is found to exist at the edge of the Brillouin zone ($q=\pi$). Figure 12 depicts a typical example of such a solution. Again, two different types of dark solitons can be obtained; one centered on a site [Fig. 12(a)] and one centered between two consecutive sites [Fig. 12(b)]. We emphasize that this family of solutions does not exist in standard arrays (as described by the DNLS equation). They are only possible in systems with appreciable second order coupling effects as, for example, in the zigzag arrays proposed here.

VII. CONCLUSIONS

In this paper we presented a method to efficiently manage the discrete diffraction properties of nonlinear waveguide arrays. As an example, we considered zigzag arrays that can provide considerable extended interactions. We demonstrated that completely different families of discrete soliton solutions are possible, which are possible over a wide range of parameters. Our method opens up opportunities for diffraction management that can be employed to generate low power spatial discrete soliton states.

[1] A. Scott, Phys. Rep. **217**, 1 (1992); O.M. Braun and Y.S. Kivshar, *ibid.* **306**, 1 (1998); S. Flash and C.R. Willis, *ibid.* **295**, 181 (1998).

[2] A.S. Davydov, J. Theor. Biol. **38**, 559 (1973); A. S. Davydov, *Biology and Quantum Mechanics* (Pergamon Press, Oxford, 1982); A.C. Scott and L. Macneil, Phys. Lett. **98A**, 87 (1983).

[3] D.N. Christodoulides and R.I. Joseph, Opt. Lett. **13**, 794 (1988).

[4] W.P. Su, J.R. Schieffer, and A.J. Heeger, Phys. Rev. Lett. **42**, 1698 (1979).

[5] A.J. Sievers and S. Takeno, Phys. Rev. Lett. **61**, 970 (1988).

[6] A. Trombettoni and A. Smerzi, Phys. Rev. Lett. **86**, 2353 (2001).

[7] H. Eisenberg, Y. Silberberg, R. Morandotti, A. Boyd, and J. Aitchison, Phys. Rev. Lett. **81**, 3383 (1998).

[8] A.B. Aceves, C.De. Angelis, T. Peschel, R. Muschall, F. Lederer, S. Trillo, and S. Wabnitz, Phys. Rev. E **53**, 1172 (1996).

[9] O. Bang and P.D. Miller, Opt. Lett. **21**, 1105 (1996).

[10] F. Lederer and J. S. Aitchison, in *Les Houches Workshop on Optical Solitons: Theoretical Challenges and Industrial Perspectives*, edited by V. E. Zakharov and S. Wabnitz (Springer-Verlag, Berlin, 1999).

[11] R. Morandotti, U. Peschel, J.S. Aitchison, H.S. Eisenberg, and Y. Silberberg, Phys. Rev. Lett. **83**, 2726 (1999).

[12] U. Peschel, R. Morandotti, J.S. Aitchison, H.S. Eisenberg, and Y. Silberberg, Appl. Phys. Lett. **75**, 1348 (1999).

[13] Y.S. Kivshar, Opt. Lett. **18**, 1147 (1993).

[14] B.A. Malomed and P.G. Kevrekidis, Phys. Rev. E **64**, 026601 (2001); P.G. Kevrekidis, K.O. Rasmussen, and A.R. Bishop, *ibid.* **61**, 2006 (2000).

[15] D.N. Christodoulides and E.D. Eugenieva, Phys. Rev. Lett. **87**, 233901 (2001).

[16] D.N. Christodoulides and E.D. Eugenieva, Opt. Lett. **26**, 1876 (2001).

[17] E.D. Eugenieva, N.K. Efremidis, and D.N. Christodoulides, Opt. Lett. **26**, 1978 (2001).

[18] H.S. Eisenberg, Y. Silberberg, R. Morandotti, and J.S. Aitchison, Phys. Rev. Lett. **85**, 1863 (2000).

[19] R. Morandotti, H.S. Eisenberg, Y. Silberberg, M. Sorel, and J.S. Aitchison, Phys. Rev. Lett. **86**, 3296 (2001).

[20] Y.S. Kivshar, W. Królikowski, and O.A. Chubykalo, Phys. Rev. E **50**, 5020 (1994).

[21] M.J. Ablowitz and Z.H. Musslimani, Phys. Rev. Lett. **87**, 254102 (2001); M.J. Ablowitz, Z.H. Musslimani, and J. Biondini, Phys. Rev. E **65**, 026602 (2002).

[22] A.W. Snyder and J.D. Love, *Optical Waveguide Theory* (Chapman and Hall, New York, 1983).

[23] D. Hennig, Eur. Phys. J. B **20**, 419 (2001).

[24] Y.S. Kivshar and D.K. Campbell, Phys. Rev. E **48**, 3077 (1993).

[25] Yu.B. Gaididei, S.F. Mingaleev, P.L. Christiansen, and K.Ø. Rasmussen, Phys. Rev. E **55**, 6141 (1997).

[26] N.G. Vakhitov and A.A. Kolokolv, Izv. Vyssh. Uchebn. Zaved., Radiofiz. **16**, 1020 (1973) [Radiophys. Quantum Electron. **16**, 783 (1973)].

[27] E.W. Laedke, K.H. Spatschek, and S.K. Turitsyn, Phys. Rev. Lett. **73**, 1055 (1994).

[28] S. Darmanyan, A. Kobyakov, E. Schmidt, and F. Lederer, Phys. Rev. E **57**, 3520 (1998).

[29] M. Johansson and Y.S. Kivshar, Phys. Rev. Lett. **82**, 85 (1998).

[30] M. Karlsson and A. Höök, Opt. Commun. **104**, 303 (1994).